


Superconductivity of non-Fermi liquids described by Sachdev-Ye-Kitaev models

Chenyuan Li , Subir Sachdev , and Darshan G. Joshi 

Department of Physics, Harvard University, Cambridge, Massachusetts 02138, USA

 (Received 16 August 2022; revised 9 November 2022; accepted 20 December 2022; published 25 January 2023)

We investigate models of electrons in the Sachdev-Ye-Kitaev class with random and all-to-all electron hopping, electron spin exchange, and Cooper-pair hopping. An attractive on-site interaction between electrons leads to superconductivity at low temperatures. Depending on the relative strengths of the hopping and spin exchange, the normal state at the critical temperature is either a Fermi-liquid or a non-Fermi liquid. We present a large- M [where spin symmetry is enlarged to $SU(M)$] study of the normal state to superconductor phase transition. We describe the transition temperature, the superconducting order parameter, and the electron spectral functions. We contrast between Fermi liquid and non-Fermi liquid normal states: we find that for weaker attractive on-site interaction there is a relative enhancement of T_c when the normal state is a non-Fermi liquid, and correspondingly a strong deviation from BCS limit. Also, the phase transition in this case becomes a first-order transition for strong non-Fermi liquids. On the other hand, for stronger on-site interaction, there is no appreciable difference in T_c between whether the superconductivity emerges from a Fermi liquid or a non-Fermi liquid. Notable features of superconductivity emerging from a non-Fermi liquid are that the superconducting electron spectral function is different from the Fermi-liquid case, with additional peaks at higher energies, and there is no Hebel-Slichter peak in the NMR relaxation rate in the non-Fermi liquid case.

DOI: [10.1103/PhysRevResearch.5.013045](https://doi.org/10.1103/PhysRevResearch.5.013045)

I. INTRODUCTION

The classic BCS theory provides a highly successful description of the onset of superconductivity (SC) from a Fermi liquid (FL). However, in modern correlated electron materials, the normal state at the onset of higher temperature superconductivity is usually not a Fermi liquid. Below the critical temperature, basic aspects of the BCS superconducting state [such as the breaking of $U(1)$ gauge symmetry by an electron pair condensate] continue to hold, but numerous quantitative details on the critical temperature, superconducting gap amplitude, and electron spectral function are not described by BCS theory.

A popular class of theories for the onset of superconductivity from a non-Fermi liquid (NFL) focus on a normal state which has a Fermi surface coupled to a critical boson [1–6]. The boson could represent a symmetry breaking order parameter at a quantum critical point, or an emergent excitation associated with spin liquid physics. This critical boson plays a dual role—it leads to the breakdown of quasiparticles in the normal state, and it also leads to superconductivity at low temperature (T) by inducing pairing between the underlying electrons. The precise manner in which the non-Fermi liquid gives way to superconductivity at low T is not well understood, and remains a topic of great interest.

In this paper, we will address the interplay between the non-Fermi liquid and superconductivity using a different class of simpler and more tractable models. These models do not have much spatial structure because of the presence of all-to-all hopping and interactions. However, they have the virtue of being exactly solvable, and so can describe the competition between the different energy scales in a quantitative manner. We consider the Sachdev-Ye-Kitaev (SYK) type of models [7,8], which are a rare class of solvable models leading to non-Fermi liquid phases [9]. Models in this class have been recently studied in different contexts of strongly correlated systems. In this work, we consider a model of electrons with an attractive on-site interaction. In the spirit of SYK models, we consider random and all-to-all hopping, exchange interaction, and Cooper-pair hopping. This model was previously considered by us and for weak interaction an anomalous metal phase (or a Bose metal) was shown to exist [10] in the proximity of superconducting phase. In this work, our focus is on the superconducting phase, and the associated thermal phase transition. Depending on the relative strength of the hopping amplitude and exchange interaction, the normal state at higher temperatures is either a FL or a NFL. Thus our model allows us to systematically investigate the emergence of superconductivity by continuously tuning between FL and NFL normal states. Moreover, we show that SC emerging from a NFL has certain unique features in the spectral function that are absent in the case of a FL-SC transition.

There have been previous studies of superconductivity in SYK models [11–19]. However, our model is distinct from the previously considered models. In our model in Eq. (18), we start with a $SU(2)$ spin symmetry [see H_j in Eq. (20)], just as in the original Sachdev-Ye (SY) model [7]. In previous

Published by the American Physical Society under the terms of the Creative Commons Attribution 4.0 International license. Further distribution of this work must maintain attribution to the author(s) and the published article's title, journal citation, and DOI.

where, initially, the role of the self-energies is to impose delta functions which define the Green's functions as two-point fermion correlators. Let us now look at the two contributions in the action. First we have

$$\begin{aligned}
 S_0 = & \int d\tau \sum_i c_{i\alpha}^\dagger(\tau) \left(\frac{\partial}{\partial \tau} - \mu \right) c_i^\alpha(\tau) + \int d\tau d\tau' \Sigma(\tau, \tau') \left[\sum_i c_{i\alpha}^\dagger(\tau) c_i^\alpha(\tau') - NMG(\tau', \tau) \right] \\
 & + \int d\tau d\tau' \frac{\Phi(\tau, \tau')}{2} \left[\mathcal{J}^{\alpha\beta} \sum_i c_{i\alpha}^\dagger(\tau) c_{i\beta}^\dagger(\tau') + NMF^*(\tau, \tau') \right] \\
 & - \int d\tau d\tau' \frac{\Phi^*(\tau, \tau')}{2} \left[\mathcal{J}_{\alpha\beta} \sum_i c^{i\alpha}(\tau) c_i^\beta(\tau') - NMF(\tau, \tau') \right].
 \end{aligned} \tag{6}$$

For the interaction terms in (4), we need to introduce additional Hubbard-Stratonovich terms which decouple the quartic fermion interactions, and then use the large M limit to replace these fields by their saddle-point values. This procedure has been carried out explicitly for a related model in Ref. [22], and we do not display the intermediate steps here. Assuming the saddle-point has $USp(M)$ symmetry, we can obtain the final answer more directly simply by the following identifications in the interaction terms:

$$c_\alpha^\dagger(\tau) c^\beta(\tau') \Rightarrow \delta_\alpha^\beta G(\tau', \tau), \quad c^\alpha(\tau) c^\beta(\tau') \Rightarrow -\mathcal{J}^{\alpha\beta} F(\tau, \tau'). \tag{7}$$

In this manner, we obtain the second contribution in the action,

$$\frac{S_1}{NM} = \frac{U}{2} \int d\tau |F(\tau, \tau)|^2 + \frac{t^2}{2} \int d\tau d\tau' [G(\tau, \tau')G(\tau', \tau) - F(\tau, \tau')F^*(\tau', \tau)]. \tag{8}$$

Now we take the variational derivative of the action with respect to G and F^* , and obtain the saddle-point equations,

$$\Sigma(\tau, \tau') = t^2 G(\tau, \tau'), \quad \Phi(\tau, \tau') = -UF(\tau, \tau)\delta(\tau - \tau') + t^2 F(\tau, \tau'). \tag{9}$$

These equations have to be supplemented by the Dyson equations obtained from the single-site action for the fermions, which follows from the first 2 spin components of the action S_0 ,

$$\mathcal{S}_c = T \sum_\omega (c_\uparrow^\dagger(i\omega), c_\downarrow(-i\omega)) \begin{pmatrix} -i\omega - \mu + \Sigma(i\omega) & \Phi(i\omega) \\ \Phi^*(i\omega) & -i\omega + \mu - \Sigma(-i\omega) \end{pmatrix} \begin{pmatrix} c_\uparrow(i\omega) \\ c_\downarrow^\dagger(-i\omega) \end{pmatrix}, \tag{10}$$

where T is the temperature. We can now write down the combined saddle point equations:

$$\begin{aligned}
 G_\Sigma(i\omega) & \equiv \frac{1}{i\omega + \mu - \Sigma(i\omega)}, \\
 \Sigma(i\omega) & = t^2 G(i\omega) = t^2 \frac{[G_\Sigma(-i\omega)]^{-1}}{|\Phi(i\omega)|^2 + [G_\Sigma(i\omega)G_\Sigma(-i\omega)]^{-1}}, \\
 \Delta & = -UT \sum_\omega \frac{\Phi(i\omega)}{|\Phi(i\omega)|^2 + [G_\Sigma(i\omega)G_\Sigma(-i\omega)]^{-1}}, \\
 F(i\omega) & = \frac{\Phi(i\omega)}{|\Phi(i\omega)|^2 + [G_\Sigma(i\omega)G_\Sigma(-i\omega)]^{-1}}, \\
 \Phi(i\omega) & = \Delta + t^2 F(i\omega).
 \end{aligned} \tag{11}$$

The normal and anomalous Green's function in the superconducting state are $G(i\omega)$ and $F(i\omega)$ along the Matsubara frequency axis, while $G_\Sigma(i\omega)$ is an intermediate quantity defined for notational convenience; $G(i\omega) = G_\Sigma(i\omega)$ only in the normal state where $\Delta = F(i\omega) = 0$.

It is useful to first solve these equations in the normal state solution by setting $\Delta = F(i\omega) = 0$, which yields for $\mu < 2t$

$$G(i\omega) \equiv G_0(i\omega) = \frac{i\omega + \mu}{2t^2} - i \frac{\text{sgn}(\omega)}{2t^2} \sqrt{4t^2 + (\omega - i\mu)^2}, \tag{12}$$

where the sign in front of the square-root is discontinuous across the real frequency axis, and is chosen so that $G_0(z) \sim 1/z$ as $|z| \rightarrow \infty$. This yields the expected semicircle density of states.

Next, we can linearize Eqs. (11) in Δ at $T > 0$ and so obtain the superconducting critical temperature T_c . We find the condition

$$1 = -UT \sum_{\omega_n} \frac{G_0(i\omega_n)G_0(-i\omega_n)}{1 - t^2 G_0(i\omega_n)G_0(-i\omega_n)}, \tag{13}$$

with ω_n a Matsubara frequency. At small $|\omega_n|$ we obtain from Eq. (12) that

$$t^2 G_0(i\omega_n)G_0(-i\omega_n) = 1 - \frac{2|\omega_n|}{\sqrt{4t^2 - \mu^2}} + \mathcal{O}(\omega_n^2). \tag{14}$$

We can now observe that the denominator in Eq. (13) has a singularity at $\omega_n = 0$, which yields the BCS log divergence.

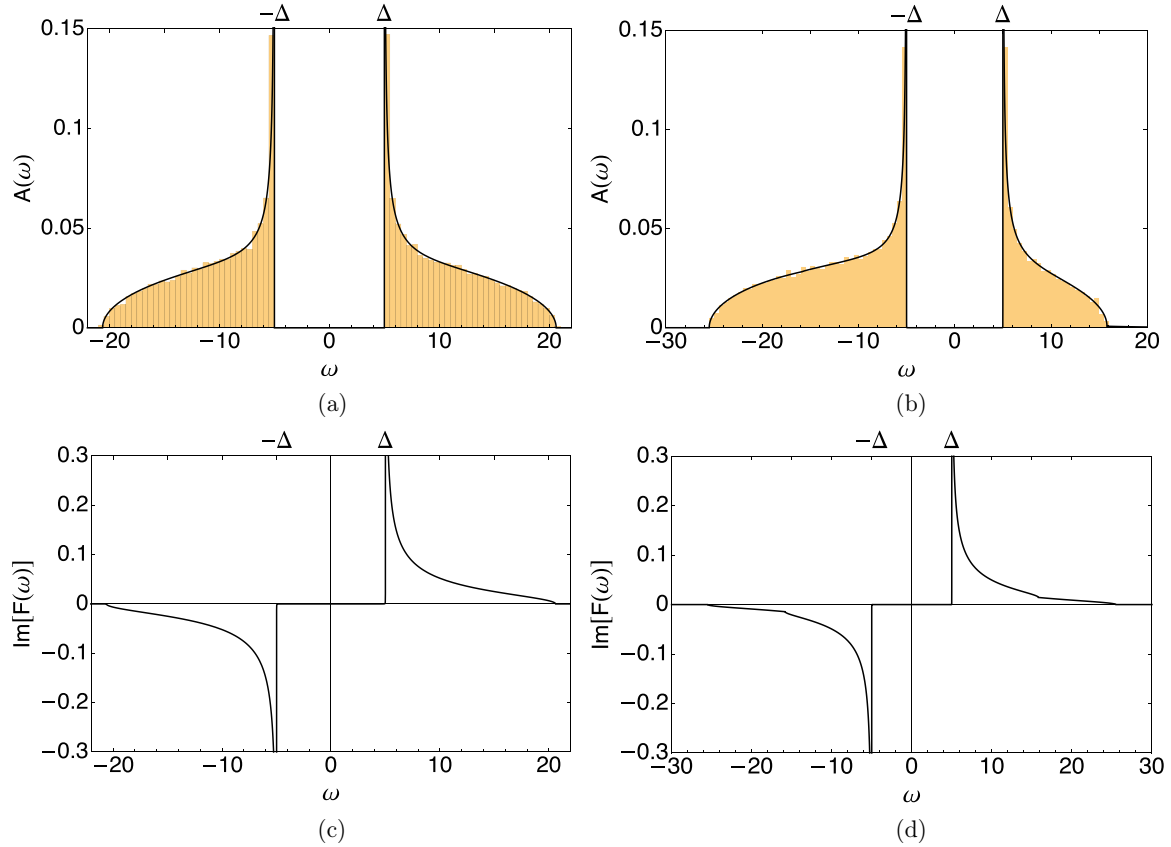


FIG. 1. (a) The spectral function, $A(\omega)$, of the normal Green's function in the SC phase at a fixed Δ for the particle-hole symmetric case ($\mu = 0$). The solid line is exact solution to the saddle point equations (11), and the yellow bars are obtained by averaging exact diagonalizations of random instances of Eq. (3). (b) Same as (a) but $\mu = 5$. (c) Imaginary part of the anomalous Green's function $F(\omega)$ in the SC phase at a fixed Δ and $\mu = 0$. (d) Same as (c) with $\mu = 5$. In all the plots, $t = 10$ and $\Delta = 5$.

This implies that there is superconductivity at $T = 0$ for infinitesimal negative U .

We can analytically solve Eqs. (11) at $T = 0$ to linear order in Δ for general μ . Such a solution will be valid for $|\omega|, \sqrt{4t^2 - \mu^2} \gg \Delta$. We find

$$F(i\omega) = \Delta \frac{(\sqrt{4t^2 + (\omega - i\mu)^2} + \sqrt{4t^2 + (\omega + i\mu)^2} - 2|\omega|)}{4|\omega|} + \mathcal{O}(\Delta^3),$$

$$G(i\omega) = G_0(i\omega) + \mathcal{O}(\Delta^2). \quad (15)$$

Note that $F(i\omega)$ is a real and even function of ω along the imaginary frequency axis. However, neither F nor G are analytic at $\omega = 0$. Similarly, we can see that $G(-i\omega) = G^*(i\omega)$, and for $\mu = 0$ $G(i\omega)$ is purely imaginary, with $G(-i\omega) = -G(i\omega)$.

At $\mu = 0$, the exact solution of the saddle-point equations in (11) is

$$G(i\omega) = -\frac{i\omega}{2t^2} \left(\frac{\sqrt{\omega^2 + 4t^2 + \Delta^2}}{\sqrt{\omega^2 + \Delta^2}} - 1 \right),$$

$$F(i\omega) = \frac{\Delta}{2t^2} \left(\frac{\sqrt{\omega^2 + 4t^2 + \Delta^2}}{\sqrt{\omega^2 + \Delta^2}} - 1 \right). \quad (16)$$

Analytic continuation gives the spectral function, $A(\omega) \equiv -\frac{1}{\pi} \text{Im}G(\omega + i\delta)$,

$$A(\omega) = \frac{|\omega|}{2\pi t^2} \frac{\sqrt{4t^2 + \Delta^2 - \omega^2}}{\sqrt{\omega^2 - \Delta^2}}, \quad \Delta < |\omega| < \sqrt{\Delta^2 + 4t^2}. \quad (17)$$

The spectral function is plotted in Fig. 1(a), along with the numerical results obtained by exact diagonalization of random realizations of the Hamiltonian in Eq. (3). As expected, the gap is centered at $\omega = 0$, between Δ and $-\Delta$. It is also straightforward to obtain the imaginary part of the retarded anomalous Green's function, which is shown in Fig. 1(c). For $\mu \neq 0$ an analytic solution is no longer possible, and we show numerical results in Figs. 1(b) and 1(d).

III. MODEL

Having discussed the basic set-up we are now ready to discuss our model. To the random Hubbard model considered in the previous section, we will now add random and all-to-all spin exchange and Cooper-pair hopping terms. So the full Hamiltonian is

$$H = H_{IU} + H_J + H_L, \quad (18)$$

$$H_{IU} = -\frac{1}{\sqrt{N}} \sum_{i < j} t_{ij} (c_{i\alpha}^\dagger c_j^\alpha + c_{j\alpha}^\dagger c_i^\alpha) + \sum_i \left[-\mu c_{i\alpha}^\dagger c_i^\alpha + \frac{U}{2M} |\mathcal{J}^{\alpha\beta} c_{i\alpha}^\dagger c_{i\beta}^\dagger|^2 \right], \quad (19)$$

$$H_J = \frac{1}{\sqrt{NM}} \sum_{i < j} J_{ij} c_{i\alpha}^\dagger c_i^\beta c_{j\beta}^\dagger c_j^\alpha, \quad (20)$$

$$H_L = -\frac{1}{2\sqrt{NM}} \sum_{i < j} L_{ij} \mathcal{J}^{\alpha\beta} \mathcal{J}_{\gamma\delta} [c_{i\alpha}^\dagger c_{i\beta}^\dagger c_j^\gamma c_j^\delta + c_{j\alpha}^\dagger c_{j\beta}^\dagger c_i^\gamma c_i^\delta]. \quad (21)$$

Recall that we have solved H_{IU} in Sec. II. H_J describes the exchange interaction of the original SY model [7], while H_L describes the random Cooper-pair hopping. In the above Hamiltonian, J_{ij} are real random numbers with zero mean

value and root-mean-square value of J . Similarly, L_{ij} can be either real or complex random numbers with zero mean value and root-mean-square value of L .

For clarity, let us consider the contribution of individual terms in the Hamiltonian in Eq. (18). The first term, H_{IU} , in Eq. (19) was already dealt with in Sec. II. Next, let us consider the contribution of H_J in Eq. (20) to the action of the full Hamiltonian. After averaging over Gaussian random variable J_{ij} the resulting action is

$$\bar{S}_J = -\frac{J^2}{4NM} \int d\tau d\tau' \left| \sum_i c_{i\alpha}^\dagger(\tau) c_i^\beta(\tau) c_{i\gamma}^\dagger(\tau') c_i^\delta(\tau') \right|^2. \quad (22)$$

In the large M limit, we can use an identity analogous to Eq. (7),

$$c_\alpha^\dagger(\tau) c^\beta(\tau) c_\gamma^\dagger(\tau') c^\delta(\tau') \Rightarrow \delta_\alpha^\delta \delta_\gamma^\beta G(\tau, \tau') G(\tau', \tau) + \mathcal{J}^{\beta\delta} \mathcal{J}_{\alpha\gamma} F^*(\tau, \tau') F(\tau, \tau'). \quad (23)$$

Here we have dropped factorizations associated with equal-time Green's functions. Then the contribution to the action from the H_J term is S_J with

$$\frac{S_J}{NM} = -\frac{J^2}{4} \int d\tau d\tau' (|G(\tau, \tau') G(\tau', \tau)|^2 + |F(\tau, \tau') F(\tau', \tau)|^2). \quad (24)$$

Finally, let us consider the contribution from the random Cooper-pair hopping term, H_L , in Eq. (21). Averaging over real Gaussian random variable L_{ij} yields the action

$$\bar{S}_L = -\frac{L^2}{8NM} \int d\tau d\tau' \mathcal{J}^{\alpha\beta} \mathcal{J}^{\mu\nu} \mathcal{J}_{\gamma\delta} \mathcal{J}_{\rho\sigma} \left[\left(\sum_i c_{i\alpha}^\dagger(\tau) c_{i\beta}^\dagger(\tau) c_i^\rho(\tau') c_i^\sigma(\tau') \right) \left(\sum_j c_{j\mu}^\dagger(\tau') c_{j\nu}^\dagger(\tau') c_j^\gamma(\tau) c_j^\delta(\tau) \right) + \left(\sum_i c_{i\alpha}^\dagger(\tau) c_{i\beta}^\dagger(\tau) c_{i\mu}^\dagger(\tau') c_{i\nu}^\dagger(\tau') \right) \left(\sum_j c_j^\gamma(\tau) c_j^\delta(\tau) c_j^\rho(\tau') c_j^\sigma(\tau') \right) \right]. \quad (25)$$

Note that the last term would be absent for complex L_{ij} . Now, we use large M identities similar to Eqs. (7) and (23), again dropping equal-time factorizations,

$$c_\alpha^\dagger(\tau) c_\beta^\dagger(\tau) c^\rho(\tau') c^\sigma(\tau') \Rightarrow (\delta_\alpha^\sigma \delta_\beta^\rho - \delta_\alpha^\rho \delta_\beta^\sigma) [G(\tau, \tau')]^2, \quad c_\alpha^\dagger(\tau) c_\beta^\dagger(\tau) c_\mu^\dagger(\tau') c_\nu^\dagger(\tau') \Rightarrow (\mathcal{J}_{\alpha\nu} \mathcal{J}_{\beta\mu} - \mathcal{J}_{\alpha\mu} \mathcal{J}_{\beta\nu}) [F^*(\tau, \tau')]^2. \quad (26)$$

The contribution of the H_L term to the action is S_L with

$$\frac{S_L}{NM} = -\frac{L^2}{4} \int d\tau d\tau' (|G(\tau, \tau') G(\tau', \tau)|^2 + |F(\tau, \tau') F(\tau', \tau)|^2), \quad (27)$$

having the same form as S_J in Eq. (24).

So finally, the action corresponding to the full Hamiltonian in Eq. (18) is

$$S = S_0 + S_1 + S_J + S_L, \quad (28)$$

with the terms S_0 and S_1 quoted in Eqs. (6) and (8), respectively, while the terms S_J and S_L are shown in Eqs. (24) and (27), respectively.

Putting everything together, the final saddle-point equations for the normal and anomalous equations are

$$G_\Sigma(i\omega) \equiv \frac{1}{i\omega + \mu - \Sigma(i\omega)}, \quad (29)$$

$$\Sigma(\tau, \tau') = t^2 G(\tau, \tau') - (J^2 + L^2) G^2(\tau, \tau') G(\tau', \tau), \quad (30)$$

$$G(i\omega) = \frac{[G_\Sigma(-i\omega)]^{-1}}{|\Phi(i\omega)|^2 + [G_\Sigma(i\omega) G_\Sigma(-i\omega)]^{-1}}, \quad (31)$$

$$\Delta = -UT \sum_\omega \frac{\Phi(i\omega)}{|\Phi(i\omega)|^2 + [G_\Sigma(i\omega) G_\Sigma(-i\omega)]^{-1}}, \quad (32)$$

$$F(i\omega) = \frac{\Phi(i\omega)}{|\Phi(i\omega)|^2 + [G_\Sigma(i\omega) G_\Sigma(-i\omega)]^{-1}}, \quad (33)$$

$$\Phi(\tau, \tau') = -UF(\tau, \tau) \delta(\tau - \tau') + t^2 F(\tau, \tau') + (J^2 + L^2) F^2(\tau, \tau') F^*(\tau', \tau). \quad (34)$$

Note that Eqs. (30) and (34) generalize the expressions in Eq. (9) upon the inclusion of the spin exchange and Cooper-pair hopping terms.

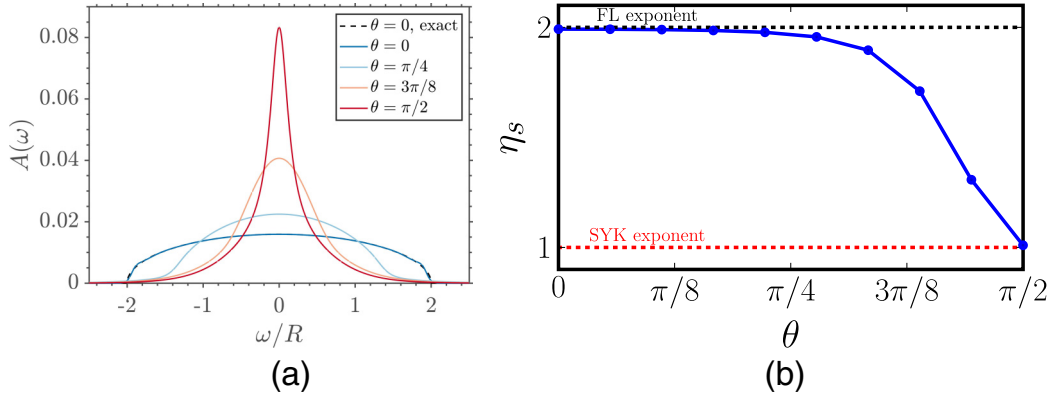


FIG. 2. (a) The normal-state spectral function $A(\omega)$ for different values of θ at $\mu = 0$, and $R/|U| = 2$. The dashed line is the exact semicircle solution for $\theta = 0$, as obtained in Eq. (12). (b) Effective spin exponent as a function of θ in the normal state at $R/|U| = 2$. The spin exponent takes the expected FL value for low θ , while it approaches the SYK value for larger θ .

IV. NUMERICAL SOLUTIONS

We shall now solve the saddle-point equations [Eqs. (29)–(34)] at finite temperature and obtain the normal-state as well as SC solutions. For simplicity and clarity, we will focus on the $\mu = 0$ half-filling case, but the results are qualitatively similar for nonzero μ as we show at the end of this section. Hence, unless otherwise stated $\mu = 0$ throughout this section. We introduce the notation $\tilde{J} = \sqrt{J^2 + L^2}$ since the interactions J and L are on equal footing in the large- M limit, as seen from Eqs. (30) and (34). Furthermore, we will parametrize the hopping t and interaction \tilde{J} as

$$t = R \cos \theta, \quad \tilde{J} = R \sin \theta, \quad (35)$$

where $R = \sqrt{t^2 + \tilde{J}^2}$, and the parameter $\theta \in [0, \pi/2]$ tunes between FL ($\theta = 0$) and SYK-NFL ($\theta = \pi/2$) limits. We will discuss results for different relative strengths with respect to U , i.e., different ratios $R/|U|$.

We solve the saddle-point equations, Eqs. (29)–(34), on the imaginary (Matsubara) frequency axis at finite temperature. The strategy is as follows. We first start with a free fermion normal Green's function, $G(i\omega_n) = (i\omega_n + \mu)^{-1}$, and a randomly chosen real function $F(i\omega_n)$, and iterate until we find a converged solution for the normal and anomalous Green's functions. The SC order parameter, $\Delta(T) = -U \mathcal{J}_{\alpha\beta} \langle c^\alpha c^\beta \rangle$, is then determined as a function of temperature. It is finite at low temperatures in the superconducting phase, and it vanishes in the normal state at higher temperature. The superconducting critical temperature T_{sc} is thus determined numerically using $\Delta(T \rightarrow T_{sc}^-) \rightarrow 0$. We will use the notation $\Delta_0 \equiv \Delta(T \rightarrow 0)$.

In both the normal and SC phases, we also compute the spectral function. The spectral function is obtained by numerical analytic continuation of Matsubara Green's functions to the real frequency axis. More details regarding numerical analytic continuation are discussed in Appendix A.

A. Normal state

The normal-state equations with $\Delta = 0$ and $F = 0$ are the same as those in Refs. [23,24]. As stated earlier, in our model we tune the parameter θ , defined in Eq. (35), to go from FL

to NFL normal states. At any given temperature T , the normal state is FL like for $\theta \lesssim \theta_{coh}$ and NFL-like for $\theta \gtrsim \theta_{coh}$, where θ_{coh} is defined by $T \sim T_{coh} = t^2/\tilde{J} = R \cos \theta_{coh} \cot \theta_{coh}$.

In Fig. 2(a), we show the spectral function in the normal state. For the FL-like phase (smaller θ), we see the expected semicircular spectral function, whereas for a NFL-like phase (larger θ) a pronounced peak at $\omega = 0$ is seen. This is consistent with earlier results obtained for a similar random model in Ref. [23].

Also, note that the FL-like normal state ($\theta < \theta_{coh}$) has the usual T^2 dependence of resistivity, while the NFL state ($\theta > \theta_{coh}$) has a linear-in- T resistivity. This is similar to the results obtained in Refs. [23,24].

The cross-over between the FL and NFL normal states can be further characterized by looking at the effective spin exponent (η_s), which is shown in Fig. 2(b). This exponent is extracted from the dynamical susceptibility, $\chi''(\omega)$, which is the imaginary part of the spin correlation. In Appendix B, we discuss the details related to the evaluation of the spin exponent η_s . Clearly, for lower values of θ the spin exponent takes the value $\eta_s = 2$ expected for a disordered FL, while in the limit $\theta \rightarrow \pi/2$, it takes the value $\eta_s = 1$ corresponding to the marginal NFL. In the intermediate θ region η_s smoothly interpolates between these extreme values. As expected, this crossover is roughly around θ_{coh} .

B. Superconducting state

Before we discuss the numerical results, we first show analytically that SC phase exists at zero temperature for any infinitesimal attractive on-site interaction. The analysis is similar to that presented in Sec. II. We determine the instability to the superconducting state by expanding the action to second order in $F(i\omega)$. This leads to the same condition for the instability as Eq. (13). However, the important difference is that the Green's function now also contains contribution from the exchange interaction terms and satisfies the equations:

$$\begin{aligned} G_0(i\omega) &= \frac{1}{i\omega + \mu - \Sigma_{el}(i\omega) - \Sigma_{in}(i\omega)}, \\ \Sigma_{el}(i\omega) &= t^2 G_0(i\omega), \\ \Sigma_{in}(\tau) &= -(J^2 + L^2)[G_0(\tau)]^2 G_0(-\tau). \end{aligned} \quad (36)$$

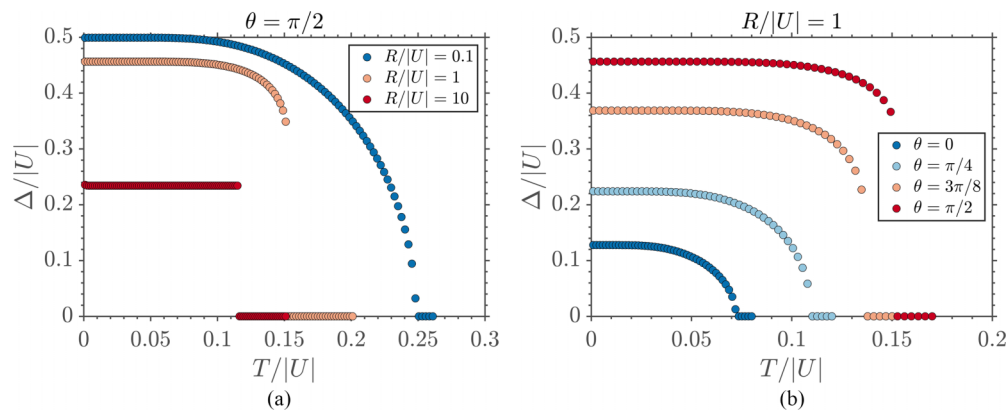


FIG. 3. SC order parameter, Δ , as a function of temperature, T . (a) SYK-NFL ($\theta = \pi/2$) case with varying $R/|U|$. Note that for larger values of $R/|U|$, the phase transition becomes first order instead of a continuous transition. (b) Here $R = |U|$ is fixed and θ is varied.

Note that we have separated the self-energy into an ‘elastic’ part Σ_{el} , and an ‘inelastic’ part Σ_{in} . This is useful because $\text{Im} \Sigma_{in}(\omega \rightarrow 0) = 0$ at $T = 0$, and that is not true for the elastic part.

From Eq. (36), we can write a quadratic equation for $G_0(0)$:

$$t^2[G_0(0)]^2 - (\mu - \Sigma_{in}(0))G_0 + 1 = 0. \quad (37)$$

An important point is that $\Sigma_{in}(0)$ is real, and so it can be absorbed into μ . This quadratic equation has two roots, and they correspond to $G_0(i0^+)$ and $G_0(i0^-)$. From the formula for the product of the roots of a quadratic equation, we can therefore conclude that at $T = 0$,

$$\lim_{\omega \rightarrow 0} G_0(i\omega)G_0(-i\omega) = \frac{1}{t^2}. \quad (38)$$

So this equation holds even when J or L are nonzero, and the denominator in Eq. (13) vanishes. Thus indicating the presence of SC at $T = 0$.

Let us now discuss the numerical results obtained by solving the saddle-point equations. For low enough temperature, we find a SC solution with a nonzero Δ and $F(i\omega)$. In Fig. 3, we have shown the variation of SC order parameter, Δ , with temperature. It turns out that for small values of θ , i.e., FL-like normal state, the SC-normal state transition is continuous. However, at larger values of θ , the phase transition (SC to NFL) becomes first order for larger values of $R/|U|$ [as seen in Fig. 3(a)]. Note that although the absolute value of Δ and T_{sc} depends on the value of U , the variation of $\Delta/|U|$ as a function of $T/|U|$ depends only on the ratio $R/|U|$. In Fig. 4, we show the variation of SC transition temperature (T_{sc}) as a function of θ for different values of $R/|U|$. For very large on-site interaction, i.e., for very small $R/|U|$ there is no difference between SC emerging from FL or NFL. This is because in this case both hopping as well as exchange interaction are subdominant. However, at larger values of the ratio $R/|U|$, i.e., weaker on-site interaction the SC transition temperature T_{sc} strongly depends on the nature of the normal state or θ . It is larger for NFL-SC transition (larger θ) as compared to the FL-SC transition (smaller θ). The same trend applies to the SC order parameter in the limit of zero temperature, Δ_0 , and the SC gap (as obtained from the spectral function) in the $T \rightarrow 0$ limit, $\tilde{\Delta}_0$, as seen in Fig. 5. Recall that in our model

SC phase corresponds to the condensation of doublon, i.e., the Cooper pairs are on the same site. A single-particle hopping tends to break these pairs and destroy SC. The exchange interaction and Cooper-pair hopping have a very weak effect in destruction of SC. Therefore, T_{sc} , Δ_0 , and $\tilde{\Delta}_0$ have very weak dependence on θ for larger on-site interaction (smaller $R/|U|$), as in this case the relative strength of hopping and spin-exchange is unimportant. On the other hand, for weaker on-site interaction the relative strength of hopping, t , compared to \tilde{J} is important. Hence for larger θ (weaker t) SC is more stable leading to a higher T_{sc} . This is also the reason why the SC-NFL transition becomes first order in nature for larger $R/|U|$.

We have also calculated the ratio $2\Delta_0/T_{sc}$ and $2\tilde{\Delta}_0/T_{sc}$, which is 3.53 for the BCS superconductivity (for FL-SC there is no difference between Δ_0 and $\tilde{\Delta}_0$ as discussed below). This is shown in Figs. 5(c) and 5(d). We find that in our case, this ratio approaches the BCS value for smaller θ (FL normal state) and weaker on-site interaction. For SC emerging from NFL normal state this ratio deviates strongly from the BCS value. The value of this ratio first increases with θ as long as the transition is continuous, and then tends to decrease as the transition changes its nature to first order. This trend follows from the observation that the transition temperature increases very sharply for large values of θ and $R/|U|$ compared to the much gradual increase in Δ_0 . In the FL case (smaller θ), both Δ_0 and T_{sc} are suppressed exponentially as a function of $R/|U|$ such that their ratio is a constant. However, in the NFL case (larger θ) this is not true anymore. Both Δ_0 and T_{sc} appear to decrease with different power-laws with respect to $R/|U|$, and in particular for larger values of θ the transition temperature T_{sc} saturates quickly for large θ . This is shown in Fig. 13 in Appendix. We have also computed the spectral function for the SC phase. This is shown in Fig. 6. As expected, we clearly see the SC gap in the spectral function. For $\theta = 0$ (FL normal state), we see the expected square-root divergence near $\omega = \Delta$. The form of this divergence seems to be modified for θ away from zero. In particular, for $\theta = \pi/2$ (SYK-NFL normal state), we see very narrow peaks. We also note that the SC gap ($\tilde{\Delta}$) observed in the spectral function may not be the same as SC order parameter Δ calculated above, as is shown in Figs. 5(a) and 5(b). The two quantities are same

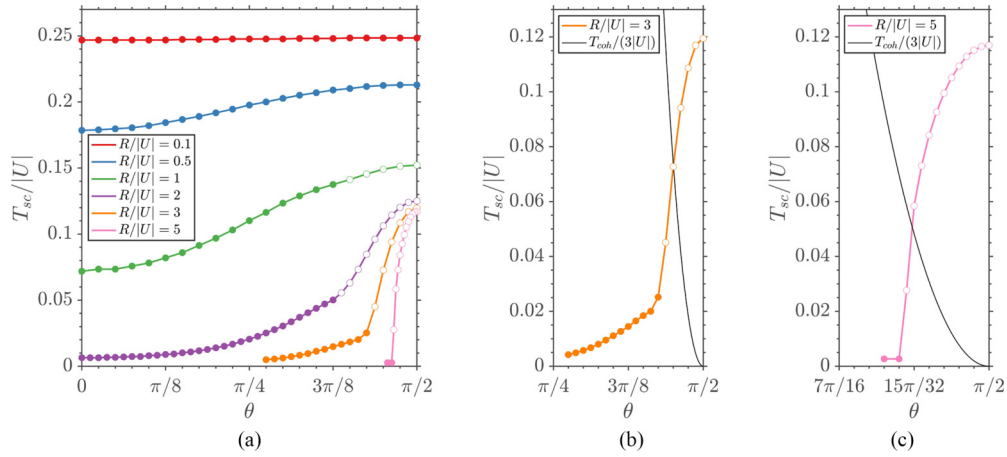


FIG. 4. (a) The SC transition temperature T_{sc} as a function of θ for different values of $R/|U|$. Qualitatively, the phase transition becomes first order (indicated by open circles) at larger values of $R/|U|$ and θ instead of a continuous transition (indicated by filled circles). (b) Comparison of T_{sc} and $T_{coh}/3 = t^2/3J = (1/3)R \cos \theta \cot \theta$ at $R/|U| = 3$. For larger values of $R/|U|$, the transition becomes first order for $\theta \gtrsim \theta_{coh}$. (c) Same as (b) but $R/|U| = 5$.

for SC emerging from FL (smaller θ), but may deviate from each other for the SC emerging from a NFL phase (larger θ). In particular, the deviation between Δ and $\tilde{\Delta}$ is strongest

for larger θ and larger values of $R/|U|$ (where the transition is of first order). In Fig. 7(a), we show the variation of the ratio of these two quantities in the limit of zero temperature,

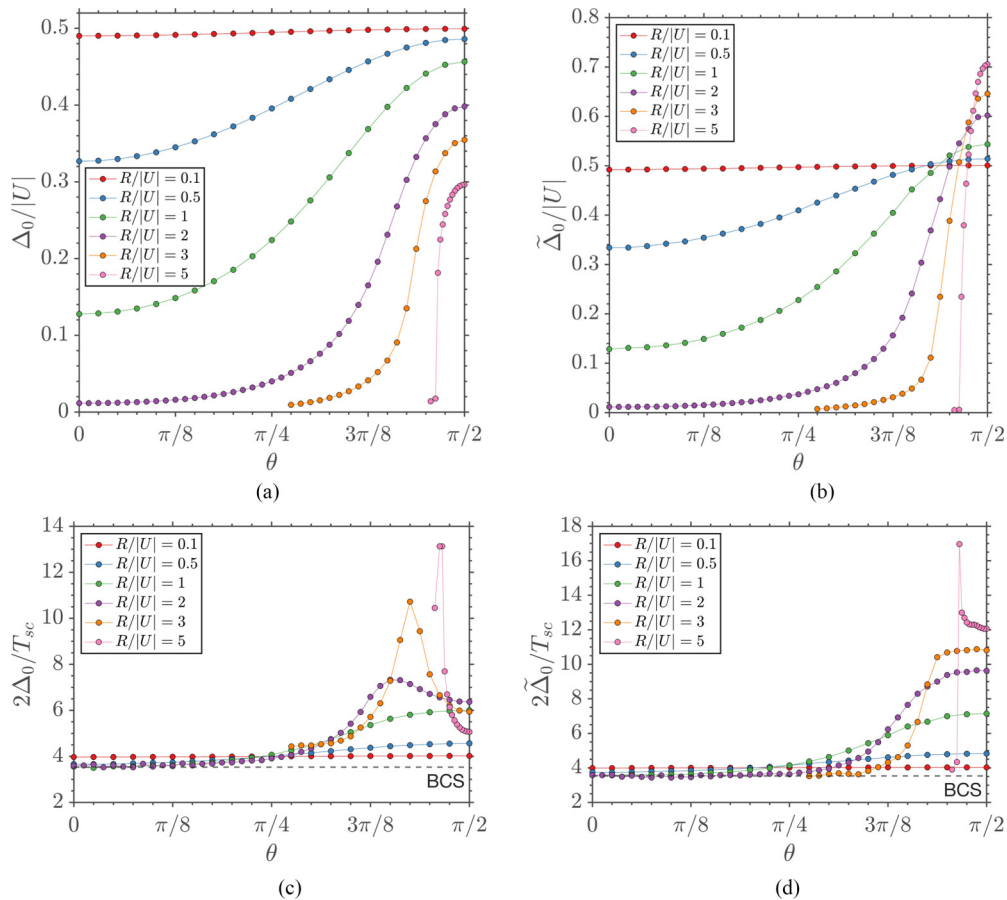


FIG. 5. (a) The variation of SC order parameter in the zero temperature limit, Δ_0 , with θ for different values of the ratio $R/|U|$. (b) The SC gap observed in the spectral function in the zero temperature limit, $\tilde{\Delta}_0$, as a function of θ . (c) The ratio $2\Delta_0/T_{sc}$. (d) The ratio $2\tilde{\Delta}_0/T_{sc}$. For larger values of θ , these ratios deviate strongly away from the BCS value of 3.53. As $\theta \rightarrow 0$ and $R/|U| \gg 1$, both $2\Delta_0/T_{sc}$ and $2\tilde{\Delta}_0/T_{sc}$ tend to the BCS result.

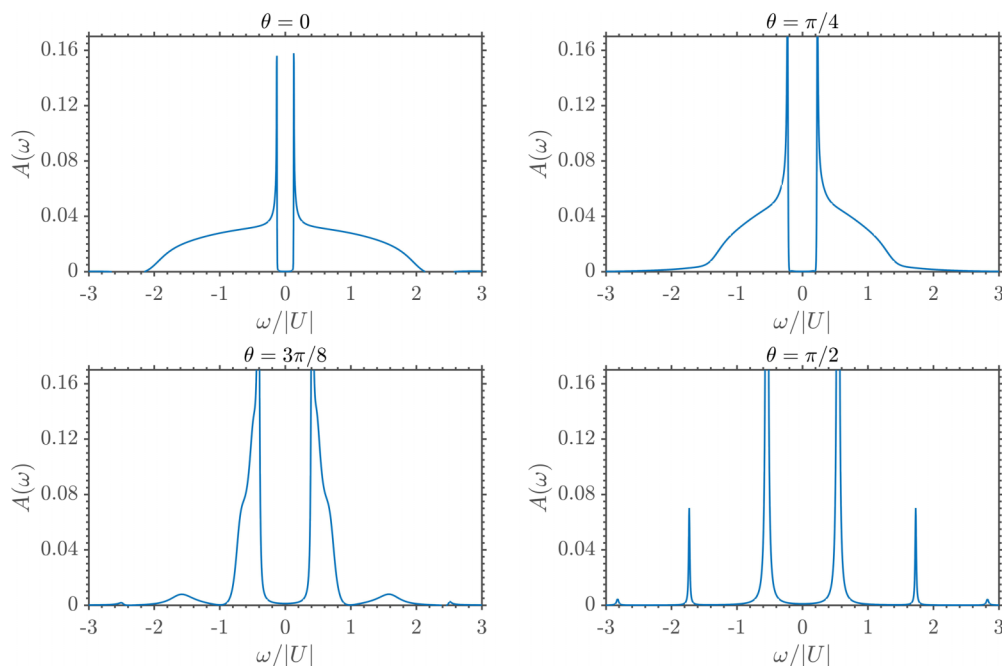


FIG. 6. The spectral functions in the superconducting phase at $R = |U|$ for different values of θ .

i.e., $\tilde{\Delta}_0/\Delta_0$, with respect to θ and $R/|U|$. We do not have an analytic expression for the gap in the spectral function, $\tilde{\Delta}$. But numerically we find that $\Delta_0 + \tilde{\Delta}_0 \simeq |U|$ at $\theta = \pi/2$, independent of the ratio $R/|U|$. This relation does not hold for other values of θ . This is shown in Fig. 7(b).

A noticeable new feature for SC emerging from NFL (larger values of θ) is the presence of peaks at higher energies compared to the SC gap [see Figs. 6(c) and 6(d)]. In the limit of $T \rightarrow 0$ the first higher-order peak appears at $\sim 3\tilde{\Delta}$. A dominant all-to-all exchange interaction (large θ) means strongly interacting Cooper pairs, which may be the reason for these additional peaks. For smaller values of θ the Cooper pairs are weakly interacting. Note that such high energy features in the spectral function have also been reported for SYK-like electron-phonon model for SC [15].

We have so far focused on the particle-hole symmetric point, $\mu = 0$, for clarity. However, it is straightforward to also do the same analysis for a nonzero chemical potential. The results are qualitatively the same as discussed above. The main difference seen is the particle-hole asymmetric distribution of the spectral weights at positive and negative frequencies, as shown in Fig. 8. The gap is however symmetric around $\omega = 0$. In the remainder of the paper, we again focus only on $\mu = 0$.

We further also compute the spin correlation in the SC phase. In Fig. 9, we plot $\chi''(\omega)$ for different values of θ in the SC phase. The features essentially follow from what was discussed for the electron spectral function earlier. The high-energy peak present in the electron spectral function at larger values of θ is also seen in $\chi''(\omega)$.

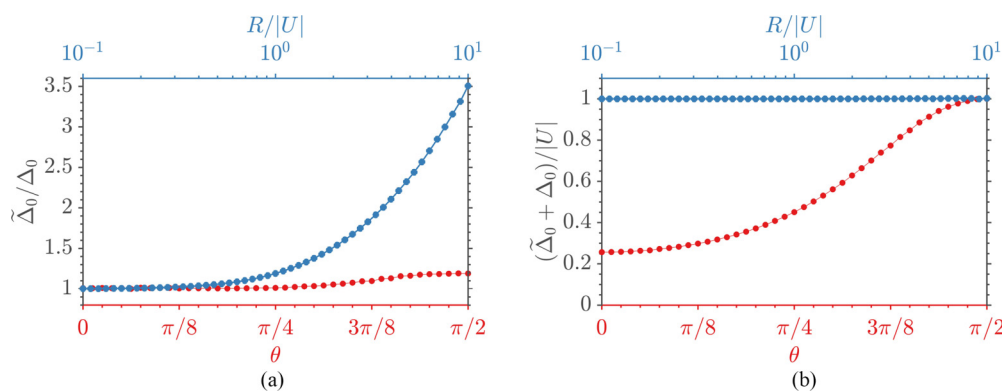


FIG. 7. (a) In the limit of zero temperature, the ratio of the SC gap, $\tilde{\Delta}_0$, (as obtained from the spectral function) and the SC order parameter, Δ_0 , as a function of $R/|U|$ at $\theta = \pi/2$ (blue) and as a function of θ at $R/|U| = 1$ (red) is shown. The two quantities are in general different away from the FL limit and for small on-site interaction the deviation between the two quantities is strongest. (b) The sum $\tilde{\Delta}_0$ and Δ_0 as a function of $R/|U|$ at $\theta = \pi/2$ (blue) and as a function of θ at $R/|U| = 1$ (red) is shown. The sum is a constant for $\theta = \pi/2$. However, this is not the case for other values of θ .

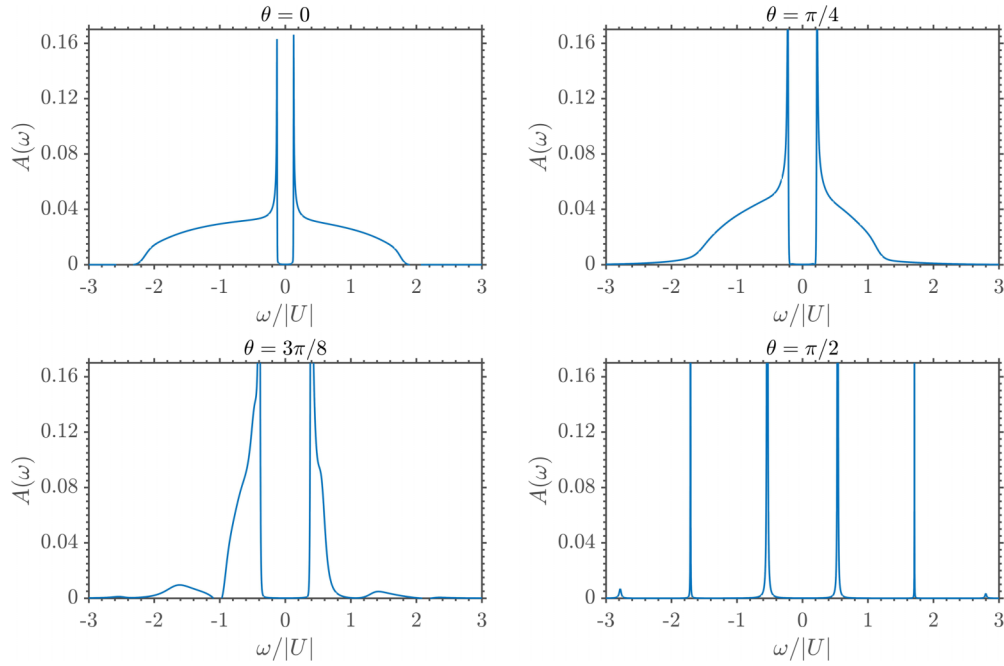


FIG. 8. The spectral functions in the superconducting phase at $R = |U|$, $\mu/|U| = 0.2$ for different values of θ .

Using $\chi''(\omega)$ we can also evaluate the temperature dependence of the NMR relaxation rate, $1/T_1$, which we show in Fig. 10. The NMR relaxation rate is given by the following relation [23]:

$$\frac{1}{T_1} = T \left. \frac{\chi''(\omega)}{\omega} \right|_{\omega=0}. \tag{39}$$

Recall that for the standard BCS superconductor one expects a peak (often referred to as the ‘‘Hebel-Slichter’’ peak) around the critical temperature as a consequence of the square-root divergence in the spectral function [25]. However, one of the signatures of the unconventional superconductivity is the absence of Hebel-Slichter peak, for instance, as observed in cuprates [26] and Fe-based superconductors [27]. We find that for a fixed $R/|U|$ when $\theta \lesssim \theta_{\text{coh}}$ there is a well distinguished

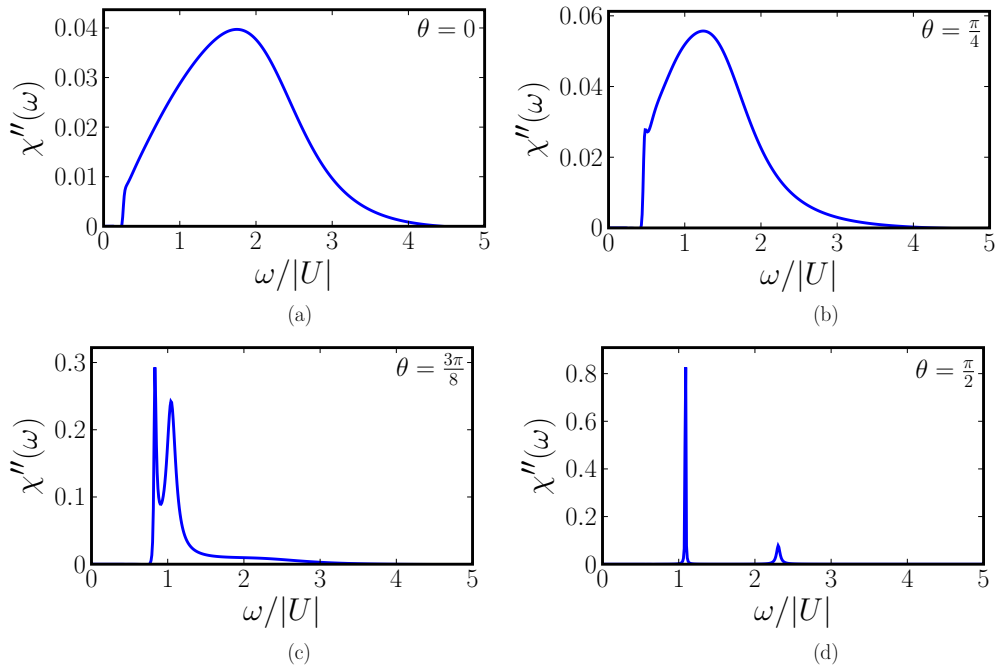


FIG. 9. Plot of imaginary part of spin correlation $\chi''(\omega)$ in the SC phase as a function of real frequency for different values of θ at $R = |U|$ and $T = 0.01$.

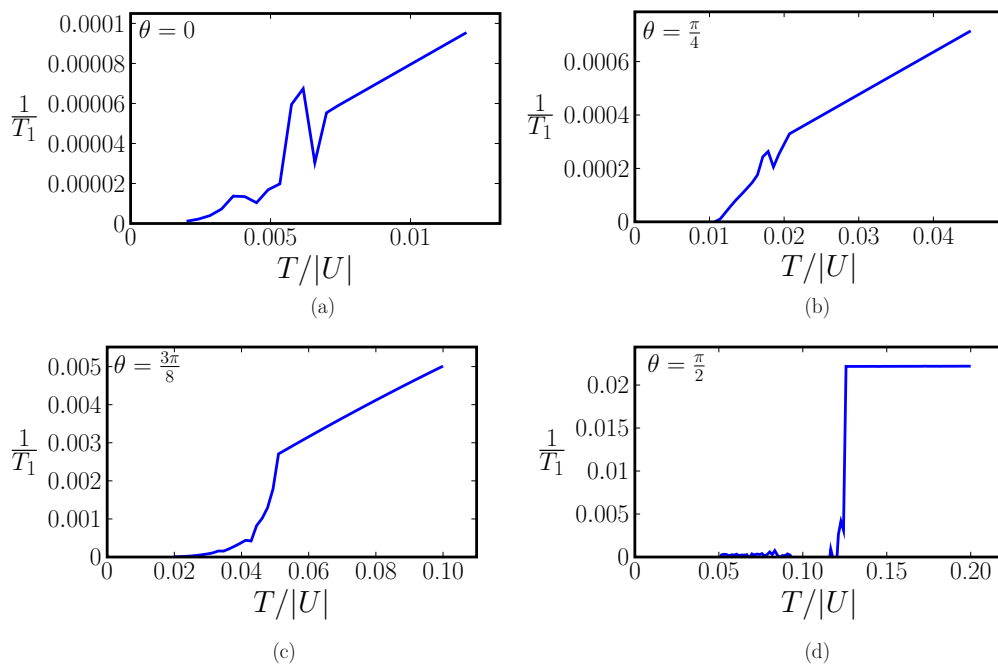


FIG. 10. Temperature dependence of the NMR relaxation rate, $1/T_1$, for different values of θ at $R = 2|U|$. Note that for smaller values of θ , where the normal state is FL-like, there is a Hebel-Slichter peak around the SC transition temperature. This can be seen in (a) around $T/|U| \sim 0.006$ and in (b) around $T/|U| \sim 0.018$, which have FL normal state. Note that the peak height diminishes as we increase θ and go closer to NFL case. The Hebel-Slichter peak is absent (and replaced by a *kink*) in case of NFL normal state, shown in (c) and (d).

Hebel-Slichter peak whose strength diminishes with increasing θ [see Figs. 10(a) and 10(b)]. After the crossover into the NFL regime for larger θ the peak is absent and there is only a *kink* around the critical temperature [see Figs. 10(c) and 10(d)]. This is another distinguishing feature between the FL and NFL cases. We also see that the relaxation rate is higher for the NFL case compared to the FL case. In the normal state this trend easily follows from the fact that the critical temperature is much higher in the NFL case. Also note that the height of the Hebel-Slichter peak present for smaller θ is roughly inversely proportional to $R/|U|$, i.e., for smaller Hubbard interaction the peak is smaller.

V. DISCUSSION

We have investigated the emergence of SC in a SYK-like model of interacting electrons, Eq. (18). The model is solved in the large- M limit, where we generalize the spin symmetry from $SU(2)$ to $SU(M)$. The solution of the large- M saddle-point equations can be viewed as a dynamical mean-field solution. We have shown the contrast between the emergence of SC from a NFL as opposed to a FL normal state. Several distinguishing features are found for SC emerging from a NFL and we summarize below the salient features of our work.

(1) Even in the presence of all-to-all and random exchange interaction and Cooper-pair hopping, we show that BCS-type superconducting instability is present, thus ensuring SC ground state at zero temperature for any infinitesimal attractive Hubbard interaction.

(2) The SC transition temperature T_{sc} is shown to be strongly enhanced for NFL normal state as compared to a FL normal state. This is an important highlight of our

results. This is understood physically by realizing that the most dominant mechanism to break Cooper pairs is single-particle hopping. However, for the NFL case, the Cooper pairs are strongly interacting, and single-particle hopping is subdominant, thus leading to a higher T_{sc} . This also renders the transition in case of NFL to be first order for weaker Hubbard interaction.

(3) While for the FL (BCS-like) case both T_{sc} and Δ are exponentially suppressed with respect to $R/|U|$, we show that for NFL case they decay with different power-laws. Consequently, the ratio $2\Delta/T_{sc}$ strongly deviates from the BCS value for SC arising from NFL.

(4) We have presented a detailed study of the local electron spectral function in the SC as well as the normal states (FL and NFL). This is an observable in photoemission experiments like ARPES. We discuss how the SC gap closes upon approaching T_{sc} . In the case of a FL normal state, the transition is continuous and BCS like, and the spectral function in SC phase features the well-known square-root divergence at $\omega = \Delta$. We show that this is not the case when the normal state is a NFL.

(5) We show that for SC emerging from a NFL there is a distinct new feature in the local electron spectral function—peaks at higher energy at $\omega \sim 3\Delta$. This is a consequence of strong interactions between Cooper pairs (which is absent in case of FL normal state). We believe that this is a generic feature of SC emerging from a NFL, and could be a relevant observation in many materials. How generic and model independent is this feature is an interesting open question for future.

(6) In the normal state, as a function of the parameter θ , there is a crossover between FL and NFL phase for a fixed

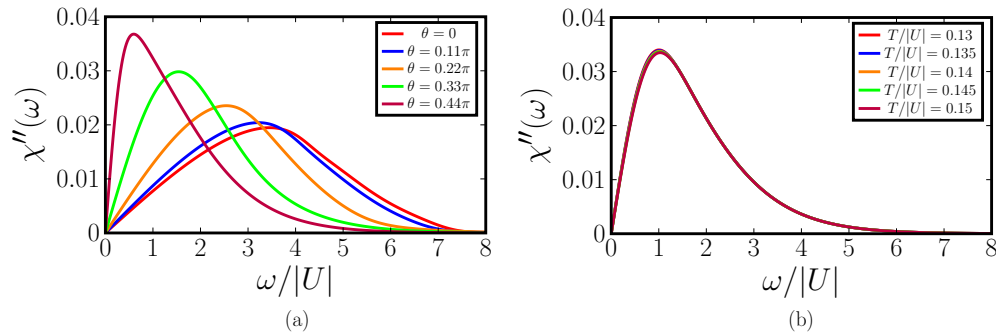


FIG. 11. (a) Plot of $\chi''(\omega)$ for different values of θ at a fixed temperature $T/|U| = 0.13$ in the normal state. (b) Plot of $\chi''(\omega)$ for different values of temperature at a fixed value of $\theta = 0.388\pi$. In both the plots, $R/|U| = 2$.

temperature, which we characterize using the effective local spin correlation exponent, η_s . The exponent deviates from FL value for $\theta \gtrsim \theta_{\text{coh}}$. We hope that our work motivates the observation of this exponent in neutron scattering experiments.

(7) We also note that NFL phase, i.e., the normal state for $\theta > \theta_{\text{coh}}$ has a linear-in-temperature resistivity. Thus SC emerging from this state may have some relevance to the situation in correlated systems.

(8) We have evaluated the local dynamic structure factor, $\chi''(\omega)$, an observable in neutron scattering experiments. In the SC phase emerging from NFL, $\chi''(\omega)$ shows distinct peaks at high energies akin to that discussed for the spectral function.

(9) Further we have also calculated the NMR relaxation rate, $1/T_1$, as a function of temperature. Here we show that for FL normal state there is a Hebel-Slichter peak near T_{sc} , which is a hallmark of BCS SC. However, for NFL case, this peak disappears and the transition temperature is marked by a *kink*. Such observations have been reported in experiments on unconventional SC in cuprates and pnictides. Our work clearly shows the mechanism for the disappearance of the Hebel-Slichter peak in the case of a NFL normal state. This may be of general relevance to the NMR experiments in unconventional SC materials.

We believe that our work will further motivate and provide a pathway to investigate SC emerging from NFL. Our work also motivates numerical investigation of the model in Eq. (18) at $M = 2$ to further elucidate the SC-NFL phase transition. We hope that our work may also provide a good starting point for constructing more realistic lattice models.

While this work was being completed, we learnt of the study Ref. [18] of essentially the same model, but with a focus on the finite N behavior.

ACKNOWLEDGMENTS

We thank G. Tarnopolsky for valuable discussions. This research was supported by the National Science Foundation under Grant No. DMR-2002850. This work was also supported by the Simons Collaboration on Ultra-Quantum Matter, which is a grant from the Simons Foundation (651440, S.S.). D.G.J. acknowledges support from the Leopoldina fellowship by the German National Academy of Sciences through Grant No. LPDS 2020-01.

APPENDIX A: NUMERICAL ANALYTIC CONTINUATION

We also perform numerical analytic continuation to real frequency. In general, performing analytic continuation is an ill-posed problem if the function on the imaginary axis is known only at a finite number of points. There are several techniques to do analytic continuation. However, for simplicity, we use the Pade approximation method. This technique parametrizes the function on imaginary axis as a ratio of two polynomials or by terminating a continued fraction. There are several ways for implementing Pade approximation. We adopt the simple strategy outlined in Ref. [28] of evaluating the coefficients of the two polynomials recursively, which is based on Thiele's reciprocal difference method. Details of the algorithm can be found in the Appendix of Ref. [28]. Briefly, we first solve the saddle-point equations on the imaginary-frequency axis to obtain the required Green's function, say $G(i\omega)$, at non-negative Matsubara frequencies. The number of Matsubara frequencies used in our calculation is 10^5 . Then we evaluate the required polynomials, $A_n(z)$ and $B_n(z)$, to approximate the imaginary-frequency function, $G(z) = A_n(z)/B_n(z)$. The accuracy of these polynomials depends on the number of Pade points, n , and in our calculation we find that $n = 200$ points are sufficient to obtain accurate results. We have checked our results by increasing or decreasing n and it does not result in any significant improvement. The resulting ratio of polynomials then corresponds to the retarded Green's function on real-frequency axis, once we identify $z = \omega +$

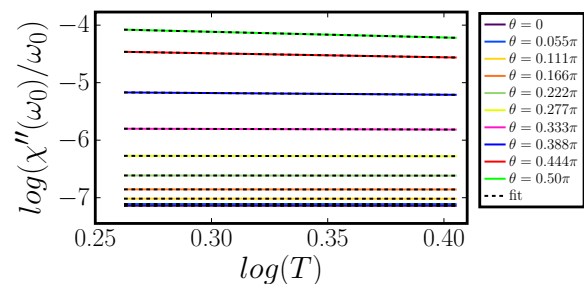


FIG. 12. Plot of $\ln(\chi''(\omega_0)/\omega_0)$ vs $\ln(T)$ at $\omega_0 = 0.2$, $R/|U| = 2$, and in the temperature range between $T/|U| = 0.13$ and $T/|U| = 0.15$, for different values of θ . The slope of the linear fit (black dashed lines) gives $\eta_s - 2$, from Eq. (B3). This is used to plot the curve of η_s as a function of θ in Fig. 2(b).

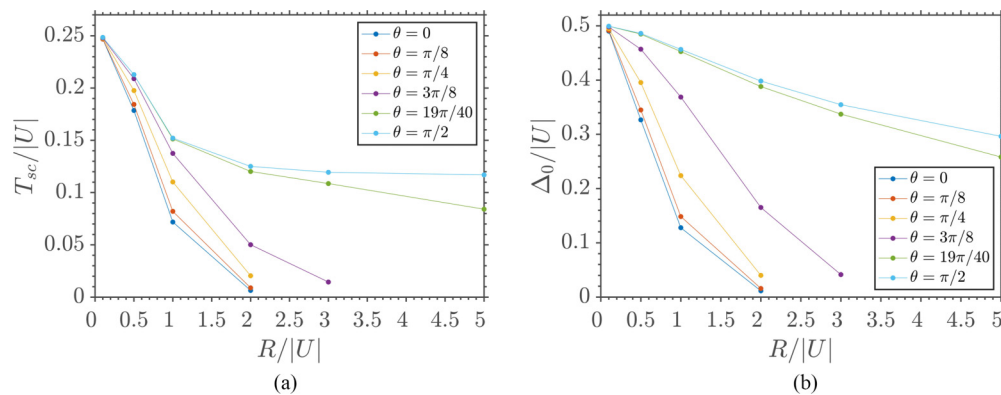


FIG. 13. Plots of transition temperature T_{sc} , the SC order parameter Δ_0 and the SC gap $\tilde{\Delta}_0$ vs R for different values of θ . Note that for smaller values of θ when the normal state is FL-like, there is an exponential decay with respect to $R/|U|$. In contrast, in the case of NFL normal state these are replaced by different power laws.

$i0^+$. Imaginary part of this function then gives the spectral function.

APPENDIX B: EFFECTIVE SPIN EXPONENT

In this Appendix, we discuss the evaluation of the effective spin exponent (η_s) in the normal state. To start with, we first evaluate the spin correlation, $\chi(\tau) = \langle \vec{S}(\tau) \cdot \vec{S}(0) \rangle \sim -G(\tau)G(-\tau)$, which is straightforward to obtain from the imaginary frequency numerics. We then Fourier transform to obtain $\chi(i\omega)$, and then perform numerical analytic continuation to obtain $\chi(\omega)$ whose imaginary part is the dynamical susceptibility, $\chi''(\omega)$. This is shown in Fig. 11 for the normal state and in Fig. 9 in the SC phase.

At temperature above the SC transition temperature, the normal state solution is one of the SYK-type conformal solutions at low energy ($\omega \ll \tilde{J}$). For such a solution, the spin susceptibility follows the scaling relation [23,29,30],

$$\chi''(\omega) \sim T^{\eta_s-1} \Phi_{\eta_s} \left(\frac{\hbar\omega}{k_B T} \right), \quad (\text{B1})$$

where

$$\Phi_{\eta_s}(y) = \sinh \left(\frac{y}{2} \right) \left| \Gamma \left(\frac{\eta_s}{2} + i \frac{y}{2\pi} \right) \right|^2. \quad (\text{B2})$$

For $\hbar\omega \ll k_B T$, we have

$$\chi''(\omega) \sim \omega T^{\eta_s-2}, \quad (\text{B3})$$

while in the limit of $\hbar\omega \gg k_B T$, the result is similar to the zero temperature form, $\chi''(\omega) \sim \text{sgn}(\omega) |\omega|^{\eta_s-1}$.

We can thus use Eq. (B3) to extract the effective spin exponent (η_s) from the slope of plot of $\ln(\chi''(\omega_0)/\omega_0)$ versus $\ln(T)$, where ω_0 is a fixed small frequency. In Fig. 12, we present the data for such a procedure for $R/|U| = 2$ in the temperature range of $T/|U| = 0.13$ and $T/|U| = 0.15$, with $\omega_0 = 0.2$. We have also checked our results for two other small frequency points, and the results are unchanged. The resulting η_s as a function of θ is plotted in Fig. 2(b). Similar procedure can be done at other values of $R/|U|$. This works well for larger values of $R/|U|$. At smaller values of $R/|U|$, the transition temperature is relatively high, where our numerical analytic continuation is not very reliable, and so extracting η_s there is difficult.

APPENDIX C: ADDITIONAL PLOTS FOR T_{sc} AND Δ

As noted earlier in the main text, the SC transition temperature (T_{sc}) and the SC order parameter (Δ_0) decay exponentially with $R/|U|$ in the case of SC emerging from FL normal state. This results in the expected BCS value for the ratio of T_{sc} and Δ_0 . However, we observe that in the case when SC emerges from a NFL normal state the transition temperature and the order parameter decay with different power-laws with respect to $R/|U|$. This is shown in Fig. 13. Deducing these power-laws analytically is an interesting problem for future work. The consequence of these power-law decay in place of an exponential is that the ratio of T_{sc} and Δ_0 is no longer a constant.

- [1] S.-S. Zhang, Y.-M. Wu, A. Abanov, and A. V. Chubukov, Interplay between superconductivity and non-Fermi liquid at a quantum critical point in a metal. VI. The γ model and its phase diagram at $2 < \gamma < 3$, *Phys. Rev. B* **104**, 144509 (2021).
 [2] D. Pimenov and A. V. Chubukov, Twists and turns of superconductivity from a repulsive dynamical interaction, *Ann. Phys.* **447**, 169049 (2022).

- [3] C. Bauer, Y. Schattner, S. Trebst, and E. Berg, Hierarchy of energy scales in an O(3) symmetric antiferromagnetic quantum critical metal: A Monte Carlo study, *Phys. Rev. Res.* **2**, 023008 (2020).
 [4] M. A. Metlitski, D. F. Mross, S. Sachdev, and T. Senthil, Cooper pairing in non-Fermi liquids, *Phys. Rev. B* **91**, 115111 (2015).

- [5] I. Mandal, Superconducting instability in non-Fermi liquids, *Phys. Rev. B* **94**, 115138 (2016).
- [6] I. Esterlis, H. Guo, A. A. Patel, and S. Sachdev, Large N theory of critical Fermi surfaces, *Phys. Rev. B* **103**, 235129 (2021).
- [7] S. Sachdev and J. Ye, Gapless Spin-Fluid Ground State in a Random Quantum Heisenberg Magnet, *Phys. Rev. Lett.* **70**, 3339 (1993).
- [8] A. Y. Kitaev, Talks at KITP, University of California, Santa Barbara, Entanglement in Strongly-Correlated Quantum Matter (2015).
- [9] D. Chowdhury, A. Georges, O. Parcollet, and S. Sachdev, Sachdev-Ye-Kitaev models and beyond: A window into non-fermi liquids, *Rev. Modern Phys.* **94**, 035004 (2022).
- [10] C. Li, D. G. Joshi, and S. Sachdev, Critical anomalous metals near superconductivity in models with random interactions, *Phys. Rev. B* **103**, 115147 (2021).
- [11] I. R. Klebanov, A. Milekhin, G. Tarnopolsky, and W. Zhao, Spontaneous breaking of U(1) symmetry in coupled complex SYK models, *J. High Energy Phys.* **11** (2020) 162.
- [12] É. Lantagne-Hurtubise, V. Pathak, S. Sahoo, and M. Franz, Superconducting instabilities in a spinful Sachdev-Ye-Kitaev model, *Phys. Rev. B* **104**, L020509 (2021).
- [13] Y. Wang, Solvable Strong-Coupling Quantum-Dot Model with a Non-Fermi-Liquid Pairing Transition, *Phys. Rev. Lett.* **124**, 017002 (2020).
- [14] H. Wang, A. L. Chudnovskiy, A. Gorsky, and A. Kamenev, Sachdev-Ye-Kitaev superconductivity: Quantum Kuramoto and generalized Richardson models, *Phys. Rev. Res.* **2**, 033025 (2020).
- [15] I. Esterlis and J. Schmalian, Cooper pairing of incoherent electrons: An electron-phonon version of the Sachdev-Ye-Kitaev model, *Phys. Rev. B* **100**, 115132 (2019).
- [16] A. A. Patel, M. J. Lawler, and E.-A. Kim, Coherent Superconductivity with a Large Gap Ratio from Incoherent Metals, *Phys. Rev. Lett.* **121**, 187001 (2018).
- [17] D. Chowdhury and E. Berg, Intrinsic superconducting instabilities of a solvable model for an incoherent metal, *Phys. Rev. Res.* **2**, 013301 (2020).
- [18] A. L. Chudnovskiy and A. Kamenev, Superconductor-insulator transition in a non-fermi liquid, [arXiv:2207.12307](https://arxiv.org/abs/2207.12307).
- [19] S. Sahoo, É. Lantagne-Hurtubise, S. Plugge, and M. Franz, Traversable wormhole and Hawking-Page transition in coupled complex SYK models, *Phys. Rev. Res.* **2**, 043049 (2020).
- [20] E. A. Yuzbashyan, A. A. Baytin, and B. L. Altshuler, Strong-coupling expansion for the pairing Hamiltonian for small superconducting metallic grains, *Phys. Rev. B* **68**, 214509 (2003).
- [21] E. A. Yuzbashyan, A. A. Baytin, and B. L. Altshuler, Finite-size corrections for the pairing Hamiltonian, *Phys. Rev. B* **71**, 094505 (2005).
- [22] M. Christos, F. M. Haehl, and S. Sachdev, Spin liquid to spin glass crossover in the random quantum Heisenberg magnet, *Phys. Rev. B* **105**, 085120 (2022).
- [23] O. Parcollet and A. Georges, Non-Fermi-liquid regime of a doped Mott insulator, *Phys. Rev. B* **59**, 5341 (1999).
- [24] X.-Y. Song, C.-M. Jian, and L. Balents, Strongly Correlated Metal Built from Sachdev-Ye-Kitaev Models, *Phys. Rev. Lett.* **119**, 216601 (2017).
- [25] L. C. Hebel and C. P. Slichter, Nuclear spin relaxation in normal and superconducting aluminum, *Phys. Rev.* **113**, 1504 (1959).
- [26] M. Takigawa, A. P. Reyes, P. C. Hammel, J. D. Thompson, R. H. Heffner, Z. Fisk, and K. C. Ott, Cu and O NMR studies of the magnetic properties of $\text{YBa}_2\text{Cu}_3\text{O}_{6.63}$ ($t_c = 62$ K), *Phys. Rev. B* **43**, 247 (1991).
- [27] H. Fukazawa, Y. Yamada, K. Kondo, T. Saito, Y. Kohori, K. Kuga, Y. Matsumoto, S. Nakatsuji, H. Kito, P. M. Shirage, K. Kihou, N. Takeshita, C.-H. Lee, A. Iyo, and H. Eisaki, Possible multiple gap superconductivity with line nodes in heavily hole-doped superconductor KFe_2As_2 studied by ^{75}As nuclear quadrupole resonance and specific heat, *J. Phys. Soc. Jpn.* **78**, 083712 (2009).
- [28] H. J. Vidberg and J. W. Serene, Solving the Eliashberg equations by means of n -point Padé approximants, *J. Low Temp. Phys.* **29**, 179 (1977).
- [29] S. Sachdev, T. Senthil, and R. Shankar, Finite-temperature properties of quantum antiferromagnets in a uniform magnetic field in one and two dimensions, *Phys. Rev. B* **50**, 258 (1994).
- [30] O. Parcollet, A. Georges, G. Kotliar, and A. Sengupta, Overscreened multichannel SU(N) Kondo model: Large- N solution and conformal field theory, *Phys. Rev. B* **58**, 3794 (1998).